Hindawi
Advances in Materials Science and Engineering
Volume 2021, Article ID 6668028, 12 pages
https://doi.org/10.1155/2021/6668028

Research Article

Study on the Dynamic Response of Gravel Soil Low Embankment under a Long-Time Dynamic Loading Based on Model Test

Dapeng Liu,[1,2,3] **Jing Wang**,[1] **and Feng Du**[2]

[1]*Jiangsu Vocational Institute of Architectural Technology, Xuzhou 221116, China*
[2]*Jiangsu Collaborative Innovation Center for Building Energy Saving and Construction Technology, Xuzhou 221116, China*
[3]*Jiangsu Engineering Laboratory of Biomass Resources Comprehensive Utilization, Xuzhou 221116, China*

Correspondence should be addressed to Dapeng Liu; 839289786@qq.com

Received 7 December 2020; Revised 6 April 2021; Accepted 12 April 2021; Published 20 April 2021

Academic Editor: Antonio Caggiano

The low embankment is an important technique for road development in subgrade engineering due to its small fill height and applicability to the natural landscape in the oasis desert area of Xinjiang, China. A reasonable development of the gravel soil low embankment design requires the study of its dynamic response under a long-time dynamic loading. In the paper, a 1 : 1 full-scale low embankment model was established and tests of 100000 loading cycles with 50 kN peak value were carried out, taking into account three kinds of foundation moisture contents: 18%, 23%, and 28%. The test results show that the dynamic stress in the gravel soil low embankment attenuates nonlinearly with the increase in depth. The dynamic stress at each depth is the smallest for the water content value of 28% in the foundation. The stress attenuation rate is inversely proportional to the loading cycles and directly proportional to the water content of the foundation. The dynamic stress and dynamic strain in the gravel soil low embankment show cumulative effects with an increase of the loading cycles. The rate of stress and strain accumulation is faster for low loading cycles. The strain accumulation effect of each structural layer in the foundation is the largest for the water content value of 28%. The strain accumulation rate at the top layer of the foundation reaches 2.648. Based on the model test results, the dynamic stress calculation model for the gravel soil low embankment under dynamic loading is proposed. The calculation model was experimentally verified. The research results are important for the application of gravel soil low embankment in the oasis desert area of Xinjiang, China.

1. Introduction

The low embankment is known for its low filling height and less impact on the ecological environment. It is the right option for road development to ensure the harmonious coexistence of humans and nature. However, the stress caused by the vehicle load cannot be effectively spread throughout the foundation and is still large. This results in a larger settlement of the foundation that leads to the early damage of the road. Thus, the service life of the road does not show the expected duration. Besides, there are no extensive studies on the dynamic response law of low embankment under long-term vehicle load, which limits their development. Through theoretical analysis, field test, model test, and numerical simulation, the studies on the response of the subgrade under load showed productive results.

1.1. Theoretical Analysis. The theoretical studies of the steady-state response of the elastic half-space under the moving point load, moving a circular uniform load, and moving rectangular uniform load at low speeds were performed by Eason [1]. Kim et al. [2] studied the response of the infinite plate on the cohesive foundation under the moving loads of varying amplitudes. Zhong et al. [3] assumed the foundation to be an elastic layered half-space body and used the method of Laplace–Hankel integral transformation and transfer matrix to derive the dynamic response formula under the action of axisymmetric load.

Based on the three-dimensional Navier equation, Lu et al. [4] established the solution model for highway subgrade and solved the dynamic response of layered foundation under traffic load using the Fourier transform technology. Based on the theory of layered elastic system, Tang et al. [5] used the complex flexibility to express the constitutive equation, established the mechanical analysis model using the transfer matrix method, and solved the dynamic stress for any depths of the viscoelastic half-space by the Laplace transformation technology. Lu et al. [6] simulated the vehicle as a multi-degree-of-freedom system, taking into account the wheel-road dynamic role, using FFT (fast Fourier transform) algorithm, and then studied the influence of dynamic wheel-pavement force, pavement unevenness, and pavement rigidity on dynamic response of embankment.

1.2. Field Test. Dai et al. [7] experimentally studied the dynamic stress of the top surface of the subgrade under the action of vehicle load for the flexible pavement. Hyodo et al. [8] used a vehicle of 100 kN axle load. Considering the static load of the vehicle and driving speeds of 10 km/h, 20 km/h, and 35 km/h, respectively, the dynamic stress values at different depths of the subgrade were obtained as the vehicle moved back and forth. Shi et al. [9] measured the dynamic stress of the subgrade in a seasonally frozen soil area. Also, the dynamic stress values at different depths of the subgrade under heavy vehicle loads were obtained to analyze the impact of vehicle load and vehicle speed. Wang et al. [10] performed the field test of the subgrade dynamic response under heavy loads. Lu et al. [11] studied the dynamic response of subgrade under heavy vehicle load through field test and analyzed the influence of axle load and vehicle speed on the result. The vertical stress and acceleration of subgrade with different depth were obtained.

1.3. Model Test. Zou et al. [12] used the model test to investigate the dynamic response of the subgrade, including the dynamic stress, dynamic strain, and dynamic displacement at different depths. Fattah et al. [13] studied the behavior of the reinforced subbase layer under cyclic loading through nine experimental models. Compared to unreinforced subbase layer, reinforced subbase layer has bigger load carrying capacity, greater failure load, and smaller settlement. Lou [14] used a self-developed separate frequency-conversion vibration exciter to carry out model test of dynamic response of subgrade and studied the dynamic response law of railway subgrade body under different excitation frequency and dynamic load level.

1.4. Numerical Simulation. Based on numerical simulations, Hall [15] analyzed the strain caused by a train in the range of subgrade and foundation using two-dimensional and three-dimensional finite element models. Fattah et al. [16, 17] established three-dimensional finite element model of plates on elastic foundation and analyzed the influence of factors on the response under impact and eccentric impact load. Li et al. [18] used the finite element method to analyze the dynamic response of railway subgrade under a dynamic load. Kong et al. [19] used finite element software to establish seven-layer track-subgrade three-dimensional numerical analysis model. The dynamic stress of the subgrade was calculated. Further, the influence of axle load and running speed on the dynamic characteristics of the subgrade was analyzed.

The low embankment has to withstand the long-term vehicle dynamic loading and the moisture content of the foundation will change in its service life cycle. So, the paper used the 1 : 1 full-scale model test to study the response of low embankment under the long-term vehicle loading. By testing the stress and strain under different conditions, the law of stress and strain of low embankment under long-term loading with depth, water content of foundation, and loading cycles was obtained. Thus, it provides a reference for the reasonable design of low embankment and the long-term stability of low embankment.

2. Model Test

2.1. Model Construction. The standard axle load adopted in China's road design code is BZZ-100, with the single axle load of 100 kN for the dual wheel group and a track width of 1.8 m. One of the wheels has little influence on the stress and strain of the subgrade and foundation under the action center of the other wheel. Thus, each wheel has an influence range of its own. Besides, the vehicle moving on the road generates waves. The wave energy of a small-sized model is not completely dissipated along the boundaries and thus affects the test results. The propagation range of the wave generated by the wheel is obtained by complex calculations. Based on this value along with a certain surplus, a full-scale model box for the influence range of a wheel was designed. The specific dimension of the model was 3 m × 1.5 m × 1.5 m.

The test model was divided into four layers, namely, the surface layer, base layer, embankment, and foundation, as shown in Figure 1. The surface layer consisted of a hot AC-16 asphalt mixture with a thickness of 0.12 m. The base layer was composed of the cement stabilized macadam, which was incorporated into the three layers of the model. The concentration of cement spread within a thickness of 0.4 m in the three layers from bottom to top was 4%, 5%, and 6%, respectively. Gravel soil was used as the subgrade filler. The thickness of the subgrade was 0.8 m, which was compacted under the optimum moisture content. Silty clay was adopted as the foundation. The thickness of the foundation was 0.7 m, which was compacted under the optimum moisture content. Coefficient of nonuniformity and coefficient of curvature were calculated through the gradation test results. Maximum dry density and optimum moisture content were measured by the compaction test. The saturated water content could be calculated by taking the soil with ring knife method and then steaming the soil when it was saturated with water. Cohesion and internal friction angle were measured by triaxial test. Resilient modulus was calculated through bearing plate test. The basic physical and mechanical parameters of gravel soil and silty clay are shown in Table 1.

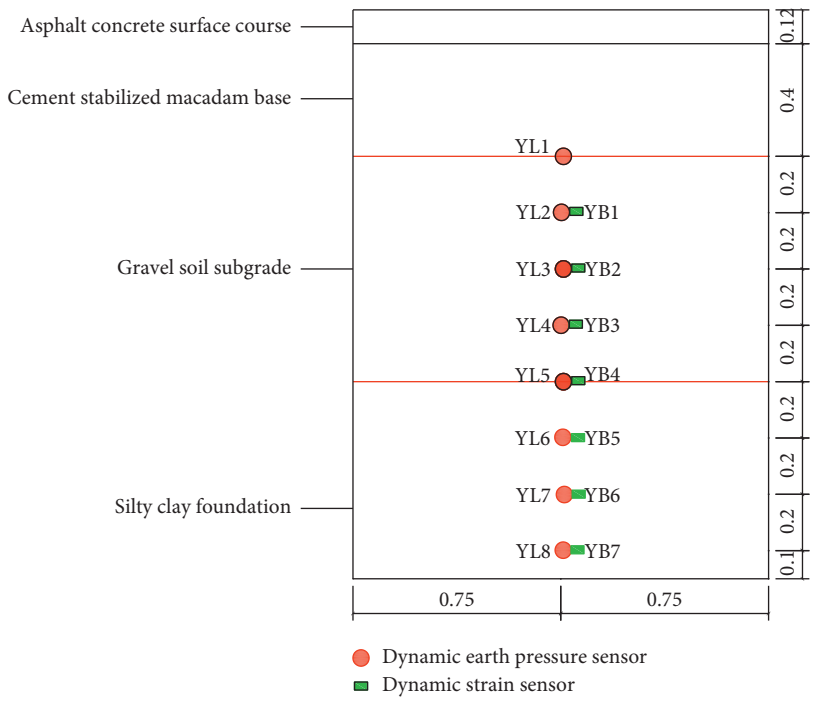

Figure 1: Model structure hierarchy and sensors layout (units in (m)).

Table 1: Basic physical and mechanical parameters of gravel soil and silty clay.

Specimen	Coefficient of nonuniformity	Coefficient of curvature	Maximum dry density (kg/m^3)	Optimum moisture content (%)	Saturated water content	Resilient modulus (MPa)	Cohesion (kPa)	Internal friction angle ( )
Gravel soil	100	1	2160	7.5	—	100	—	—
Silty clay	—	—	1725	18	28%	30	20	10

2.2. Test Equipment. The five layers of stress sensors and four layers of strain sensors were arranged within the subgrade. The upper and lower layers were 0.2 m apart. The resistance dynamic earth pressure sensor was used as the stress sensor. The embedded strain sensor was used as the strain sensor. These were connected using the whole bridge. The three-layer stress sensors and three-layer strain sensors were arranged within the scope of the foundation. The upper and lower sensors were 0.2 m apart. The specific arrangement is shown in Figure 1. From top to bottom, the stress sensors were denoted as YL1–8. The strain sensors were denoted as YB1–7. The synergy dynamic data acquisition instrument was used for data acquisition.

2.3. Loading Equipment. The channel Servo Tester System (MTS) was used for loading, as shown in Figure 2. The channel servo testing machine (MTS) is mainly composed of a hydraulic source, servo loading actuator, and control system. The loading range is 0–100 kN. The loading frequency range is 0–10 Hz. This generates loading signals of different waveforms through the control system programming.

Based on the measured results for the vehicle response to the subgrade and pavement upon motion along the road [9, 10, 20], the waveform of the vehicle load on the pavement is found to be similar to the half-sine wave. Thus, this model test used half-sine wave as the load waveform.

2.4. Test Plan. During the service life of the road, the state of the foundation often changes as a result of the change in the groundwater level and the infiltration of surface water. The state of the foundation can be simulated by changing the moisture content of the foundation. For the model test in this study, the moisture contents of the foundation were 18%, 23%, and 28%. In the model tests, 18%, 23%, and 28% were used as the optimum moisture content, unsaturated moisture content, and saturated moisture content. The compaction foundation, the unsaturated foundation, and the saturated foundation were simulated, respectively.

In the current road design code of China, the standard axle load used is the double wheel group single axle with an axle load size of 100 kN, where one side is 50 kN, and the tire grounding pressure is 0.7 MPa. This model test simulated the loading on one side of the wheel with a peak load size of

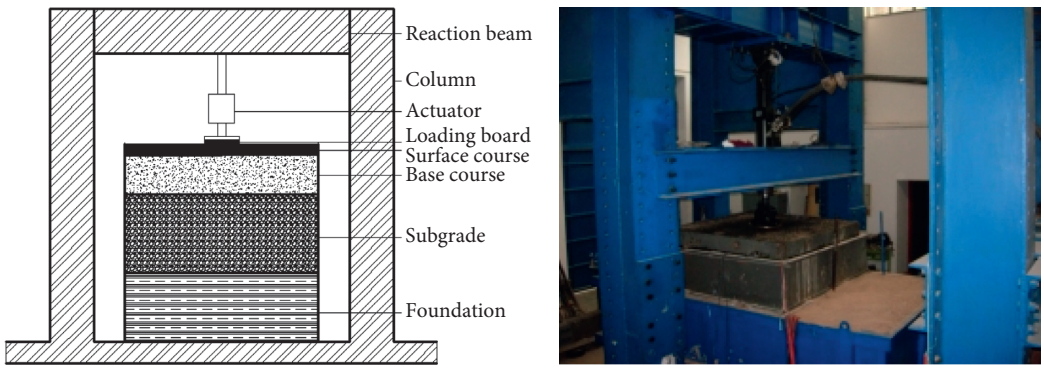

Figure 2: MTS load system. (a) Load device model diagram. (b) Actual drawing of the loading device.

50 kN. The loading plate was a single circle of 0.302 m diameter. This simulated the grounding area of one side of the tire. The loading frequency is related to the driving speed and traffic flow of the vehicle load. The loading frequency of the model test was 3 Hz and loading cycles were 100000. The specific test scheme is shown in Table 2.

3. Analysis of the Dynamic Response Test Results

3.1. Stress. The peak stress values at different depth were determined as the moisture contents of the foundation are 18%, 23%, and 28%, and the loading cycles were 100, 10000, 20000, 30000, ..., 100000, respectively. Result of 100 loading cycles was taken as the initial value. To reduce the fluctuation of the data, when determining the peak stress at each depth of 100 loading cycles, the average value of the peak stress at each depth of 1–100 loading cycles was taken. Similarly, the peak stress at each depth should be taken as the loading cycles were 10000–100000. For example, the peak stress at each depth of 10000 loading cycles was taken to be the average of the peak stress values at each depth when loading cycles were 9950–10050. When the moisture contents of the foundation were 18%, 23%, and 28%, the relationships between the stress and depth, as the loading cycles from 100 to 100000, are as shown in Figure 3.

Also, the relationships between the stress and loading cycles at each depth were plotted, as shown in Figure 4. It was concluded from Figures 3 and 4 that the stress decreased nonlinearly with an increase in depth under the moisture content values of 18%, 23%, and 28% for the foundation and fixed loading cycles. This is because the stress diffuses downward and the diffusion area increases continuously, which leads to a continuous decrease in stress.

The stress attenuation rate was defined as the ratio of the upper layer stress after subtracting the lower layer stress to the upper layer stress for fixed loading cycles. Based on the test results, the stress attenuation rate of the three values of foundation moisture content under different loading cycles could be calculated. The results are shown in Figure 3.

It can be seen from Table 3 that the stress attenuation rate decreases as a whole with the increase of loading cycles for a fixed value of water content in the foundation, even though the change in rate is low. The attenuation rates corresponding to the three values of moisture content decrease to a certain extent as loading cycles increase from 10000 to 100000. When the loading cycle is fixed, the stress attenuation rate increases with the increase in the water content of the foundation. The stress attenuation rate corresponding to 28% moisture content in the foundation is greater than that of 18% and 23% moisture content.

It was also concluded from Figures 3 and 4 that the stress at each depth decreased with the increases of water content in the foundation for a fixed loading cycle. When the moisture content of foundation was 18%, the stress was the largest. When the moisture content of foundation was 28%, the stress was the minimum.

With the increase of loading cycles, the stress at each depth increased. This showed that the stress at each depth had a certain cumulative effect with the loading cycles increase. This is attributed to the longer release time of the dynamic stress in the subgrade and foundation compared to the time interval of the dynamic load. Thus, the dynamic stress in each subgrade and foundation cannot be fully released and accumulated. The stress accumulation rate was defined as the ratio of difference between the stress of each depth at a certain loading cycle and the initial stress to the initial stress. The cumulative stress rates of the top surface of the subgrade under different loading cycles for the moisture content values of 18%, 23%, and 28% in the foundation are shown in Table 4.

It is seen from Figure 4 and Table 4 that the stress accumulation rate at the top of the subgrade was fast, especially for the first 20000 loading cycles, for small loading cycles. The stress accumulation rate gradually decreased with the increase of loading cycles. The stresses at other depths also changed in the same way.

3.2. Strain. The strain in this paper refers to the average strain in a certain range of depth. When the loading cycles were 100, 10000, 20000, 30000, ..., 100000, the peak strain of each structural layer in the subgrade and foundation was the same as that of the stress. To reduce the fluctuation of the data, when determining the peak strain of each structural

Table 2: Test scheme.

Moisture content of foundation (%)	Peak load/kN	Frequency/Hz	Loading cycles
18	50	3	100k
23	50	3	100k
28	50	3	100k

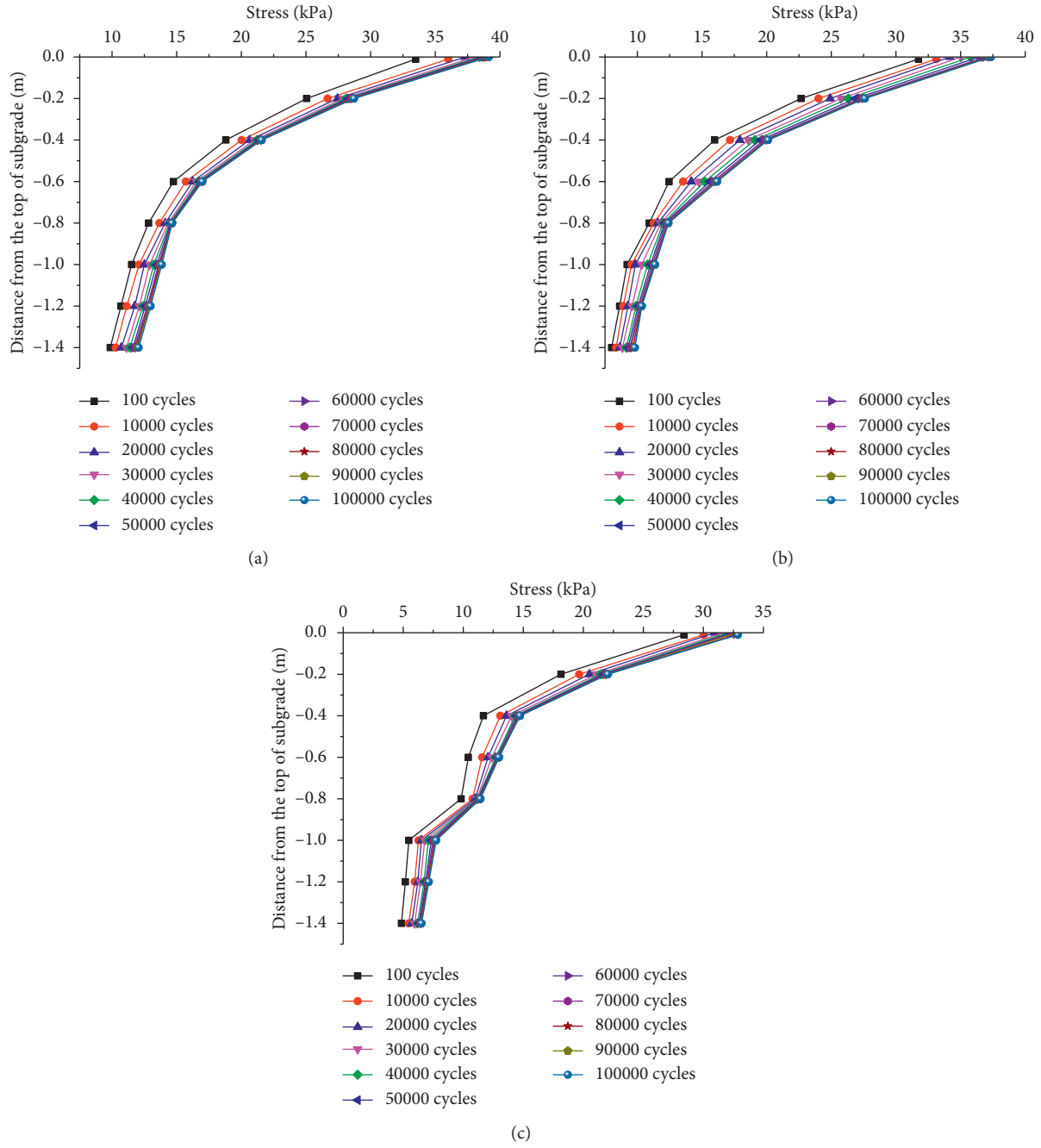

Figure 3: The relationships between stress and depth under different loading cycles. (a) The moisture content of the foundation was 18%. (b) The moisture content of the foundation was 23%. (c) The moisture content of the foundation was 28%.

layer of 100 loading cycles, the average value of the peak strain of each structural layer of 1–100 loading cycles was taken. Similarly, the peak strain of each structural layer should be taken as the loading cycles were 10000–100000. For example, the peak strain of each structural layer of 10000 loading cycles was taken to be the average of the

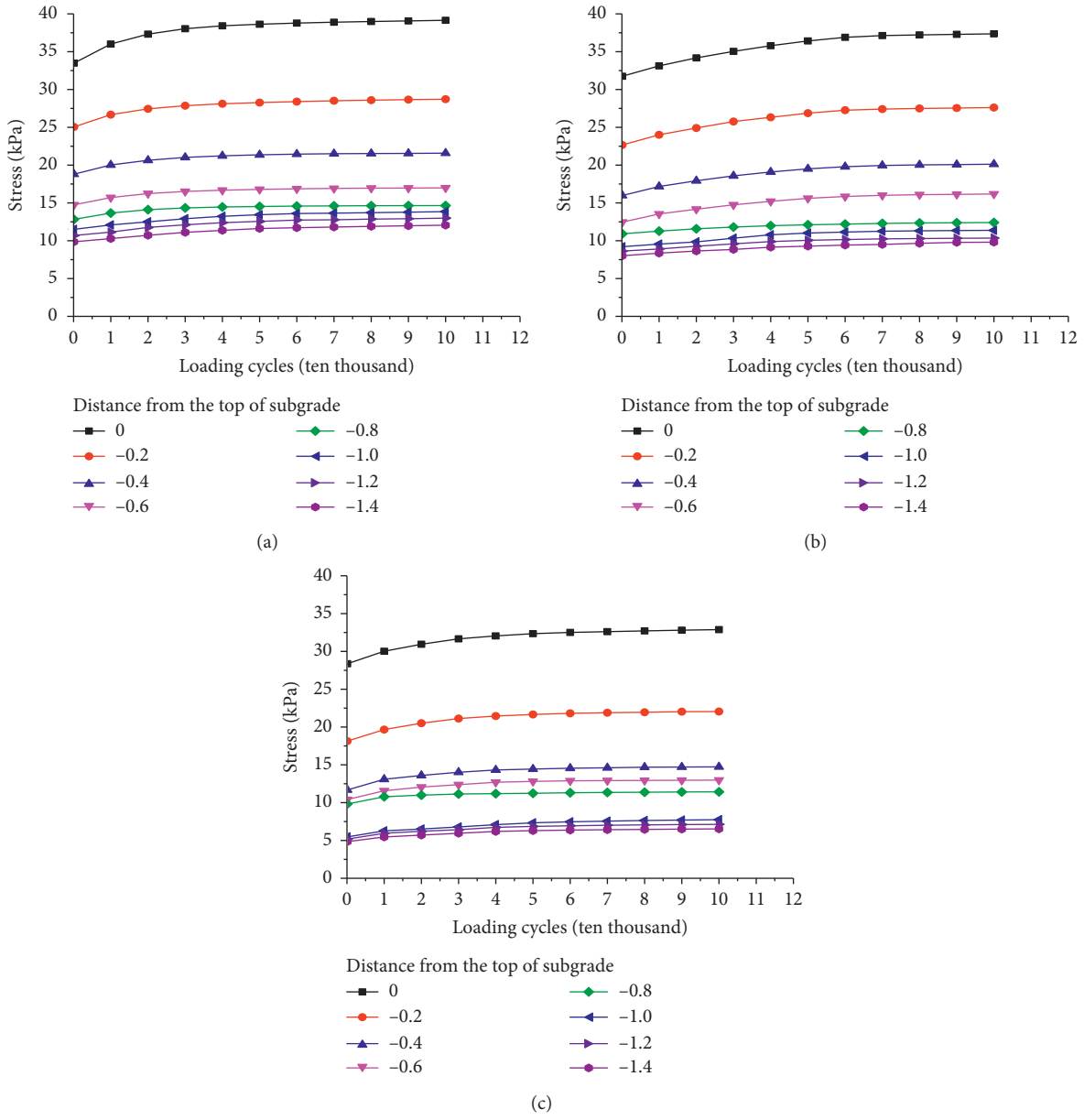

Figure 4: The relationships between stresses and loading cycles at different depths. (a) The moisture content of the foundation was 18%. (b) The moisture content of the foundation was 23%. (c) The moisture content of the foundation was 28%.

Table 3: Stress attenuation rate in the test range under different loading cycles.

	Loading cycles									
Moisture content of foundation	10k	20k	30k	40k	50k	60k	70k	80k	90k	100k
18	0.715	0.713	0.708	0.704	0.699	0.698	0.696	0.695	0.693	0.692
23	0.748	0.747	0.747	0.744	0.745	0.745	0.744	0.740	0.738	0.737
28	0.818	0.816	0.812	0.807	0.805	0.804	0.803	0.803	0.802	0.801

peak strain values of each structural layer when loading cycles were 9950–10050. The relationships between the strains and depths of each structural layer were plotted for the corresponding values of 18%, 23%, and 28%, respectively, for the water content of the foundation and under the different dynamic loading cycles, as shown in Figure 5. Also, the relationship curves between the strains of each structure layer and the loading cycles for the three values of soil moisture content are shown in Figure 6.

Table 4: Cumulative stress rate of subgrade top under different loading cycles.

	Loading cycles									
Moisture content of foundation	10k	20k	30k	40k	50k	60k	70k	80k	90k	100k
18	0.075	0.114	0.136	0.147	0.153	0.158	0.162	0.164	0.167	0.169
23	0.043	0.077	0.104	0.127	0.147	0.162	0.169	0.172	0.174	0.177
28	0.058	0.091	0.116	0.130	0.140	0.146	0.149	0.153	0.157	0.159

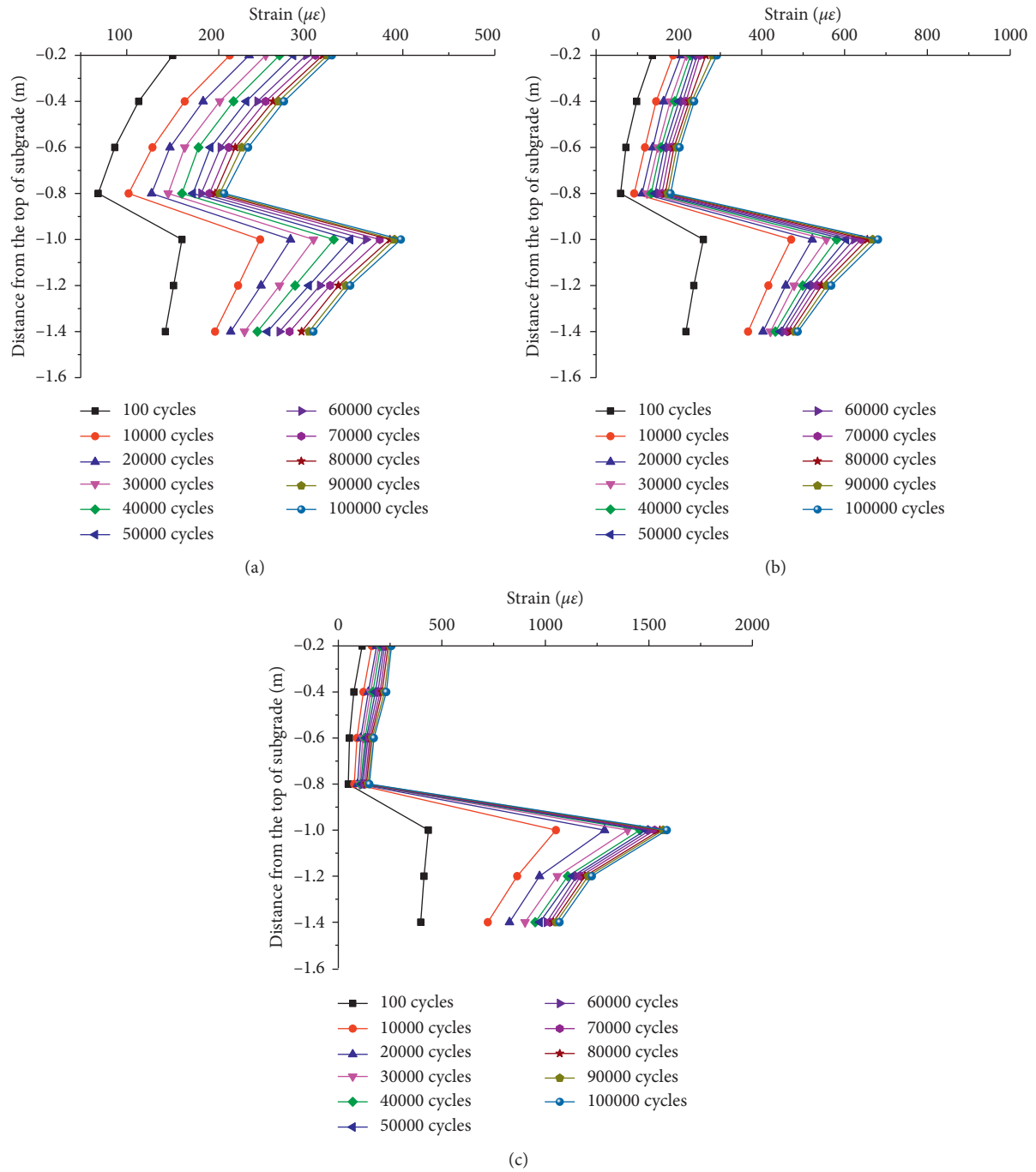

Figure 5: The relationships between strains and depths of each structural layer under different loading cycles. (a) The moisture content of the foundation was 18%. (b) The moisture content of the foundation was 23%. (c) The moisture content of the foundation was 28%.

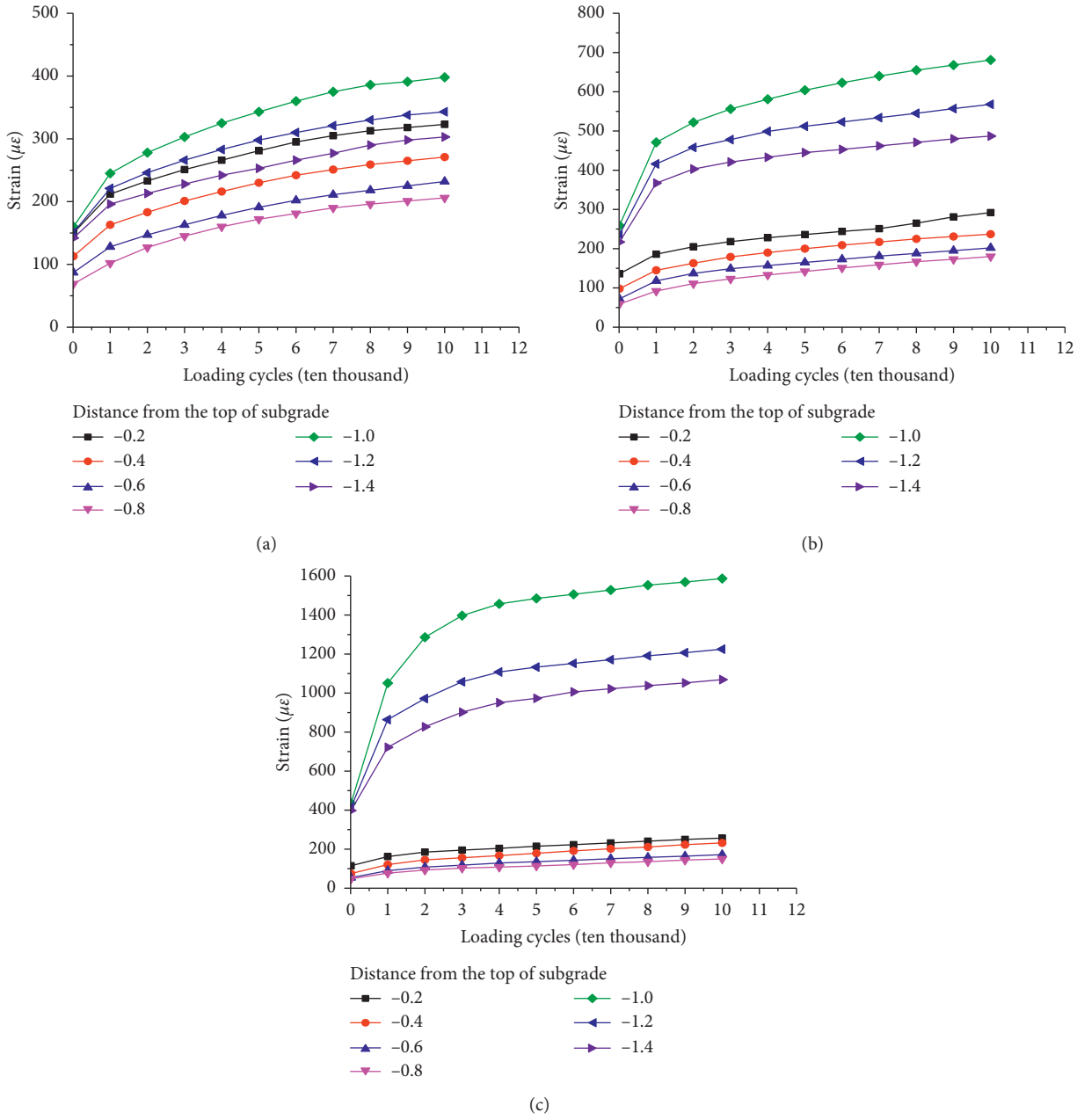

Figure 6: The relationship between the strains of different structural layers and loading cycles. (a) The moisture content of the foundation was 18%. (b) The moisture content of the foundation was 23%. (c) The moisture content of the foundation was 28%.

It could be seen from Figures 5 and 6 that the strains of each structural layer within the subgrade range decreased gradually with the increase in depth for a fixed loading cycle. This is due to the nonlinear decrease in stress with the increase in the depth, while the strength of the subgrade is constantly maintained. The strains of each structural layer in the range of foundation followed the same trend. Although the stress in the range of the foundation was less than that in the subgrade, the strain in the foundation was greater than that in the range of the subgrade for a fixed loading cycle. This was attributed to the lower strength of the foundation compared to that of the subgrade. It was also seen from Figures 5 and 6 that the strains of each structural layer accumulated similar to the stress with the increase of loading cycles. This was due to the continuous increase in stress accumulation leading to a continuous increase in the plastic strain. The strain cumulative rate was defined as the ratio of the difference between the strain of a layer at a certain loading cycle and the initial strain to the initial strain. The strain accumulation rates within 0.2 m of the top layer of the subgrade and 0.2 m of the top layer of the foundation under different loading cycles were determined, as shown in Tables 5 and 6.

From Tables 5 and 6 and Figure 6, it could be concluded that the strain increased rapidly for small loading cycles. This was especially observed before 10000 loading cycles, which

Table 5: Strain accumulation rate within 0.2 m of the top layer of the subgrade.

	Loading cycles									
Moisture content of foundation	10k	20k	30k	40k	50k	60k	70k	80k	90k	100k
18	0.413	0.553	0.673	0.773	0.873	0.967	1.033	1.087	1.120	1.153
23	0.368	0.507	0.603	0.676	0.735	0.794	0.846	0.949	1.066	1.147
28	0.409	0.609	0.696	0.774	0.870	0.939	1.017	1.096	1.174	1.235

Table 6: Strain accumulation rate within 0.2 m of the top layer of the foundation.

	Loading cycles									
Moisture content of foundation (%)	10k	20k	30k	40k	50k	60k	70k	80k	90k	100k
18	0.531	0.738	0.894	1.031	1.144	1.250	1.344	1.413	1.444	1.488
23	0.819	1.015	1.147	1.243	1.332	1.405	1.471	1.529	1.579	1.629
28	1.416	1.956	2.211	2.349	2.414	2.462	2.513	2.570	2.607	2.648

correspond to the fastest increment. With the increase of loading cycles, the rate of increase in the strain of each structural layer decreased. For a fixed loading cycle, the strain accumulation rate of each structural layer in the subgrade range was smaller than that in the foundation range. The cumulative effect of the strain was more pronounced as the water content of the foundation increased. Although the dynamic stress within the range of the water content was smaller, the settlement deformation was the largest, which was attributed to the minimum strength of the foundation.

4. Calculation Model for the Dynamic Stress of Gravel Soil Low Embankment under Long-Term Dynamic Loading

4.1. Calculation of Dynamic Stress at the Top of the Subgrade. The accurate calculation of the dynamic stress of low embankment under long-term vehicle loading is the basis for the determination of road settlement and stability. Thus, it is highly significant to determine the dynamic stress calculation model of the low embankment under long-term dynamic loading. Based on the change rule of dynamic stress in the model test, the calculation model of the dynamic stress accumulation σ_1 at the top of the subgrade under long-term dynamic loading was proposed, as shown in the following formula:

$$\sigma_1 = \sigma_0 \times \frac{aN^b}{1 + cN^b}, \tag{1}$$

where σ_0 is the initial dynamic stress at the top of the subgrade, σ_1 is the accumulated value of dynamic stress after N vehicle loading cycles, N is loading cycles, and a, b, and c are the parameters related to the factors such as pavement structure layer, foundation state, the peak value of vehicle loading, subgrade filler, and vehicle loading cycles.

The dynamic stress accumulation model parameters a, b, and c of the top surface of the subgrade could be calculated via programming under the moisture content values of 18%, 23%, and 28% of the foundation and loading cycles of 100000. The corresponding dynamic stress accumulation model for the top surface of the subgrade could be expressed by formulas (2)–(4), respectively.

When the moisture content of the foundation was 18%,

$$\sigma_1 = \sigma_0 \times \frac{0.025 \times N^{0.654}}{1 + 0.021 \times N^{0.654}}. \tag{2}$$

When the moisture content of the foundation was 23%,

$$\sigma_1 = \sigma_0 \times \frac{0.6 \times N^{0.158}}{1 + 0.345 \times N^{0.158}}. \tag{3}$$

When the moisture content of the foundation was 28%,

$$\sigma_1 = \sigma_0 \times \frac{0.168 \times N^{0.408}}{1 + 0.135 \times N^{0.408}}. \tag{4}$$

The moisture content of the foundation was 18%, 23%, and 28%, respectively, for the above three calculation models. The dynamic stress values at the top surface of the subgrade under different loading cycles were calculated and compared with the measured values, as shown in Figure 7. From Figure 7, it was seen that the measured values of dynamic stress at the top of the subgrade were close to the calculated value according to formula (1) with a difference of less than 5% for the three values of foundation water content. This indicated that formula (1) could be used to calculate the dynamic stress at the top of the low embankment under different dynamic loading cycles.

4.2. Calculation of Dynamic Stress at Any Depth. According to the variation rule of dynamic stress measured by the model at different depths, it was proposed that the dynamic stress σ at any depth could be obtained from the accumulated dynamic stress σ_1 and attenuation coefficient η at the top of the subgrade for a fixed loading cycle. The corresponding formula was as follows:

$$\sigma = \sigma_1 \times \eta. \tag{5}$$

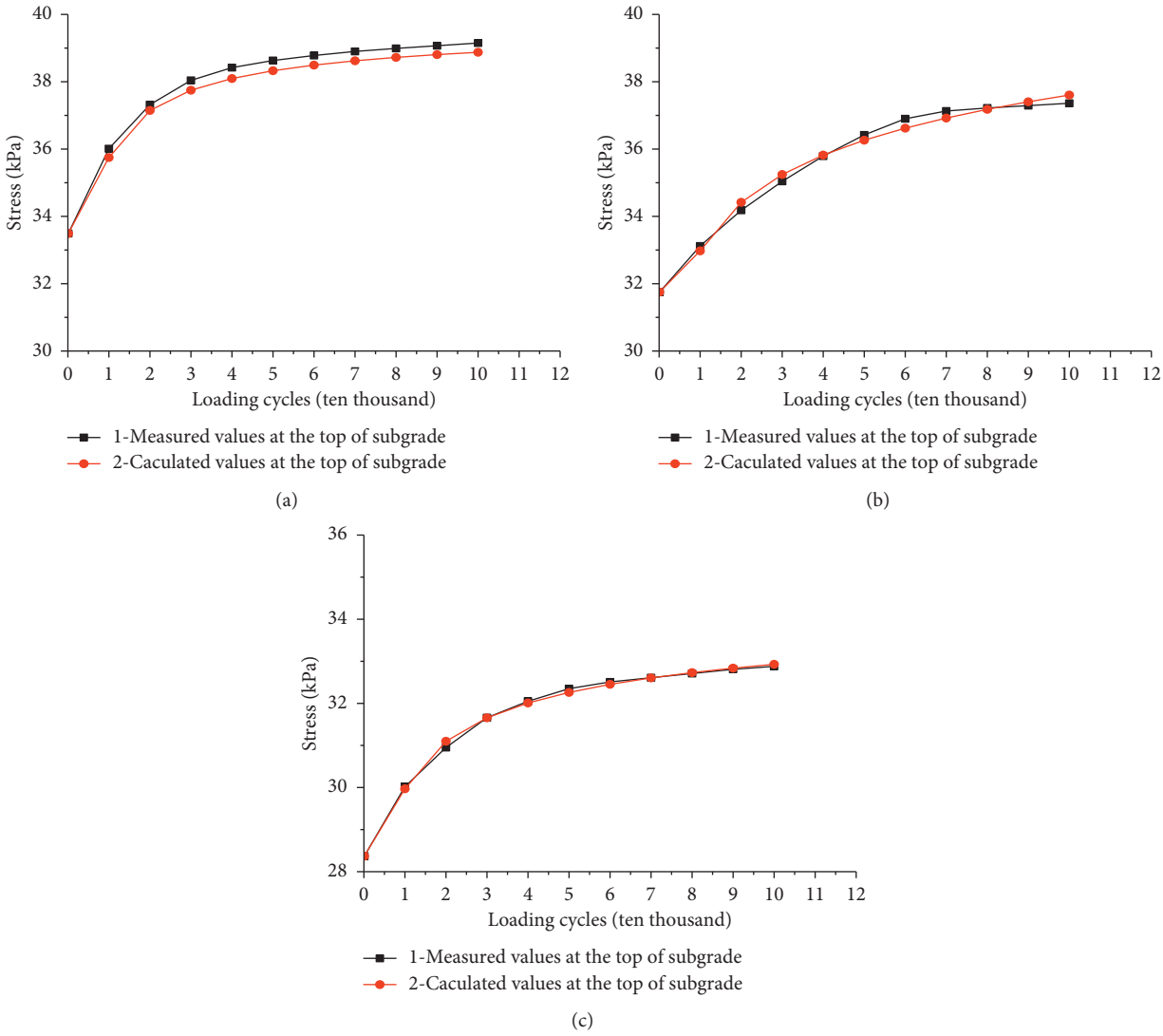

Figure 7: Comparison between the calculated and measured values of dynamic stress at the top of the subgrade under different loading cycles. (a) The moisture content of the foundation was 18%. (b) The moisture content of the foundation was 23%. (c) The moisture content of the foundation was 28%.

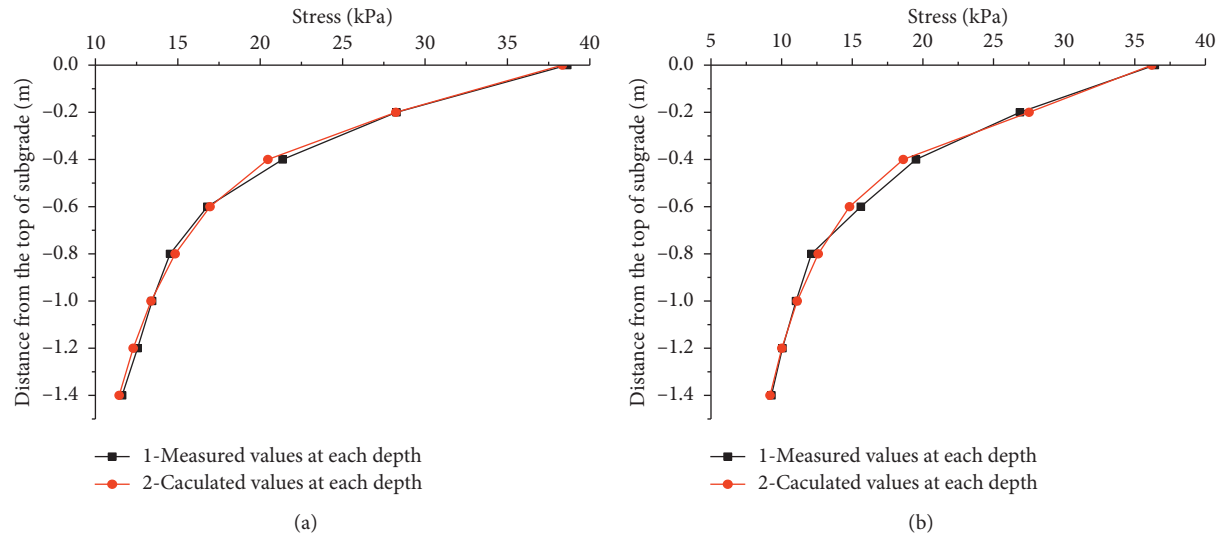

Figure 8: Continued.

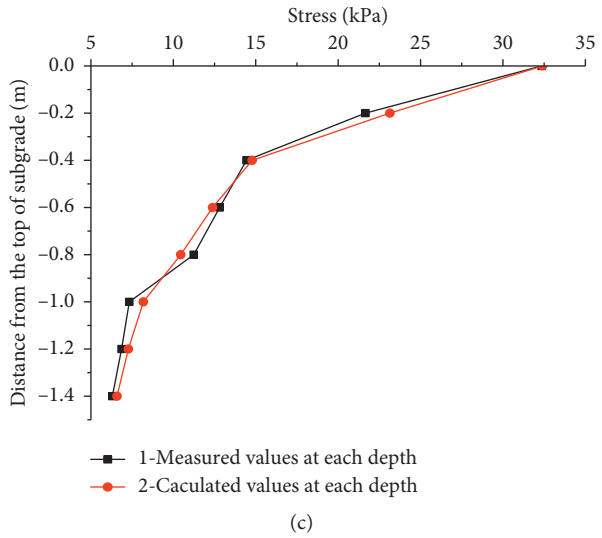

Figure 8: Comparison between the calculated and measured values of dynamic stress at each depth of 50000 loading cycles. (a) The moisture content of the foundation was 18%. (b) The moisture content of the foundation was 23%. (c) The moisture content of the foundation was 28%.

In (5), the attenuation coefficient η could be obtained using

$$\eta = \xi z^{\psi}, \tag{6}$$

where z is the distance from the top surface of the subgrade and ξ and ψ are the coefficients related to the thickness of the structural layer, material, and other parameters.

Formulas (1), (5), and (6) were used to calculate the dynamic stress σ_z at any depth of the low embankment under different dynamic loading cycles.

$$\sigma_z = \xi z^{\psi} \times \sigma_0 \times \frac{aN^b}{1 + cN^b}. \tag{7}$$

Formula (7) was used to calculate the dynamic stress at each depth of the low embankment under the water content values of 18%, 23%, and 28% of the foundation as the loading cycles were 50000. The comparison between the calculated and measured values of the model test is shown in Figure 8. Legends 1, 3, and 5 correspond to the measured values of dynamic stress for the three values of foundation water content. Legends 2, 4, and 6 correspond to the calculated values of dynamic stress for the three values of foundation water content.

From Figure 8, it was concluded that the measured value of dynamic stress at different depths was in good agreement with the value calculated using formula (7) with a difference of about 10% as the dynamic loading cycles were 50000. Therefore, formula (7) could be used to calculate the dynamic stress at any depth in the low embankment under different dynamic loading cycles.

5. Conclusions

(1) For fixed vehicle loading cycles, the stress at each depth of the gravel soil low embankment decreased nonlinearly with the increase in depth. The stress at the same depth decreased as the water content of the foundation increased. The stress attenuation rate slightly decreased with the increase of vehicle loading cycles for a fixed value of water content in the foundation. For fixed vehicle loading cycles, the stress attenuation rate increased with the increase of water content of the foundation.

(2) Under the long-term vehicle loading, the stress and strain in the subgrade and foundation showed cumulative effects. The cumulative rate of stress and strain was faster for smaller loading cycles. With the increase of loading cycles, the cumulative rate of stress and strain decreased.

(3) The accumulation effect of strain in each structural layer was more pronounced as the water content of the foundation increased. When the water content of the foundation was 28%, the strain accumulation rate at the top layer of the foundation reached 2.648.

(4) The dynamic stress at any depth is obtained by multiplying the dynamic stress at the top of the subgrade with the attenuation coefficient for fixed loading cycles. The dynamic stress at the top of the subgrade σ_1 is obtained using the cumulative calculation model in this paper.

(5) Based on the specific low embankment structure, the phenomena of stress accumulation and strain accumulation are obtained from the model test results. The law of stress and strain accumulations of other low embankment structures will be studied in the future. The values of parameters a, b, c, ξ, and ψ need to be determined from the experimental data.

Data Availability

The data used to support the findings of this research are included within the paper.

Conflicts of Interest

The authors declare that there are no conflicts of interest regarding the publication of this paper.

Acknowledgments

The authors gratefully acknowledge the supports for this work provided by major projects of Natural Science Foundation of Jiangsu Provincial Department of Education (18KJA560001), Doctoral Program of JiangSu Collaborative Innovation Center for Building Energy Saving and Construction Technology (SJXTBS1706), Xuzhou Science and Technology Project (KC17156), Jiangsu Construction System Science and Technology Project (2017ZD085), Scientific Research Project of Jiangsu Vocational Institute of Architectural Technology (SJXTY1508), and Jiangsu Qinglan Project.

References

[1] G. Eason, "The stresses produced in a semi-infinite solid by a moving surface force," *International Journal of Engineering Science*, vol. 2, no. 6, pp. 581–609, 1965.

[2] S.-M. Kim and B. F. Mccullough, "Dynamic response of plate on viscous winkler foundation to moving loads of varying amplitude," *Engineering Structures*, vol. 25, no. 9, pp. 1179–1188, 2003.

[3] Y. Zhong, J. Chen, L. Wang et al., "Xplicit solution for dynamic response of axisymmetrical problems in multilayered viscoelastic half space," *Chinese Journal of Computational Mechanics*, vol. 20, no. 6, pp. 749–755, 2003.

[4] Z. Lu, H. L. Yao, X. W. Luo et al., "3D dynamic responses of layered ground under vehicle loads," *Rock and Soil Mechanics*, vol. 30, no. 10, pp. 2965–2970, 2009.

[5] L. S. Tang, P. Y. Lin, K. Wu et al., "Response characteristics of dynamic stress of subgrade soil under vehicle loads," *Chinese Journal of Geotechnical Engineering*, vol. 33, no. 11, pp. 1745–1749, 2011.

[6] Z. Lu, Z. Hu, H. Yao, J. Liu, and Y. Zhan, "An analytical method for evaluating highway embankment responses with consideration of dynamic wheel-pavement interactions," *Soil Dynamics and Earthquake Engineering*, vol. 83, pp. 135–147, 2016.

[7] S. Dai and D. Van Deusen, "Field study of in situ subgrade soil response under flexible pavements," *Transportation Research Record: Journal of the Transportation Research Board*, vol. 1639, no. 1, pp. 23–35, 1998.

[8] M. Hyodo, K. Yasuhara, and H. Murata, "Deformation analysis of the soft clay foundation of low embankment road under traffic loading," in *Proceeding of the 31st Symposium of Japanese Society of Soil Mechanics and Foundation Engineering*, vol. 27–32, Tokyo, Japan, 1996.

[9] F. Shi, J. K. Liu, J. H. Fang et al., "Subgrade dynamic stress test on highway in seasonal frozen soil area," *China Journal of Highway and Transport*, vol. 25, no. 5, pp. 15–20, 2013.

[10] X. Wang, J. H. Zhang, G. Y. Yang et al., "Test on dynamic stress of roadbed and pavement under heavy loads," *Journal of Vibration and Shock*, vol. 26, no. 6, pp. 169–173, 2007.

[11] Z. Lu, Z. Hu, H.-L. Yao, and J. Liu, "Field evaluation and analysis of road subgrade dynamic responses under heavy duty vehicle," *International Journal of Pavement Engineering*, vol. 19, no. 12, pp. 1077–1086, 2018.

[12] J. R. Zou, Z. Y. Li, and X. W. Cao, "Research of the dynamic performance of the full weathering granite subgrade and pavement by model test," *Journal of Highway and Transportation Research and Development*, vol. 24, no. 4, pp. 58–62, 2007.

[13] M. Y. Fattah, A. S. Aladili, and H. F. Yousif, "Behavior of reinforced sub-base layer on dried expansive soil under cyclic loading," *Journal of Earth Sciences and Geotechnical Engineering*, vol. 7, no. 3, pp. 23–49, 2017.

[14] S. Lou, "In-situ dynamic experimental study for simulating dynamic response of subgrades," *Chinese Journal of Rock Mechanics and Engineering*, vol. 39, no. 3, pp. 629–636, 2020.

[15] L. Hall, "Simulations and analyses of train-induced ground vibrations in finite element models," *Soil Dynamics and Earthquake Engineering*, vol. 23, no. 5, pp. 403–413, 2003.

[16] M. Y. Fattah, M. J. Hamood, and S. A. Abbas, "Behavior of plate on elastic foundation under impact load," *Engineering and Technology Journal*, vol. 32, no. 4, pp. 1007–1027, 2014.

[17] M. Y. Fattah, M. J. Hamood, and S. A. Abbas, "Dynamic response of plates on elastic foundation under eccentric impact load," in *International Conference on Advances in Sustainable Construction Materials & Civil Engineering Systems (ASCMCES-2017)*, August 2017.

[18] J. S. Li and K. C. Li, "Finite element analysis for dynamic response of roadbed of highspeed railway," *Journal of the China Railway Society*, vol. 17, no. 1, pp. 66–75, 1995.

[19] X. H. Kong, G. L. Jiang, A. H. Li et al., "Analysis of dynamic characteristics of railway subgrade based on three-dimensional numerical simulation," *Journal of Southwest Jiaotong University*, vol. 49, no. 3, pp. 406–411, 2014.

[20] J. M. Zhao, S. Y. Liu, M. L. Shi et al., "Experimental study on dynamic response of low embankment under traffic load," *Journal of Southeast University (Natural Science Edition)*, vol. 37, no. 5, pp. 921–925, 2007.